Int. J. Electrochem. Sci., 14 **(2019)** 10931 – 10942, doi: 10.20964/2019.12.28

International Journal of
ELECTROCHEMICAL
SCIENCE
www.electrochemsci.org

A Novel Pt/WC_x/C Electrocatalyst Synthesized by a One-Pot Method for Methanol Electrooxidation in Acid Media

Xiaowei Zhang[‡], *Tianyu Ai*[‡], *Chang Ma*, *Jinlin Lu*[*]

School of Materials and Metallurgy, University of Science and Technology Liaoning, Anshan 114051, P. R. China.
[*]E-mail: lujinlin@ustl.edu.cn
[‡] These authors contributed equally to this work

Received: 3 August 2019 / *Accepted:* 13 September 2019 / *Published:* 29 October 2019

The development of new electrocatalysts with low platinum (Pt) loading and high electrochemical activity is still a challenge for fuel cell technologies. In this work, novel electrocatalysts, Pt nanoparticles alloyed with tungsten carbide (WC) supported on nanocarbon materials (Pt/WCx/nanocarbon), were synthesized by a newly developed one-pot method for the methanol oxidation reaction (MOR) in direct methanol fuel cells (DMFCs). The so-called one-pot method has two key steps. First, Pt-containing ligands and W-containing ligands were self-assembled on nanocarbon materials, namely, carbon nanotubes or carbon black. Second, the products obtained from the first step were freeze-dried. The composition and structure of the Pt/WC_x/nanocarbon electrocatalysts were characterized by several testing means, such as X-ray diffraction, field emission scanning electron microscopy, transmission electron microscopy, and X-ray photoelectron spectroscopy. The results showed that Pt and WC were alloyed when their ratio was in an appropriate range. The electrochemical performances for the MOR were evaluated by cyclic voltammetry and chronoamperometry in acid media. The results showed that the Pt/$WC_{0.15}$/C electrocatalyst displayed the highest electrocatalytic activity and the best stability for MOR. The enhancements in electrochemical performance are attributed to the negative shift of the d-band centre of elemental Pt, which can weaken the adsorption strength towards CO molecules, facilitate the removal of the CO groups and improve MOR activity. The newly developed one-pot method has a great deal of potential for synthetizing Pt and carbide nanocomposite electrocatalysts and demonstrates a broad prospect in the application of fuel cells.

Keywords: Electrocatalyst; Self-assembly; Methanol oxidation reaction; Tungsten carbide; One-pot method

1. INTRODUCTION

Many researchers have made tremendous efforts in the development of renewable energy due to the increasing energy demand in modern society [1-3]. As portable power sources, direct methanol

fuel cells (DMFCs) have been widely researched worldwide [4-7]. In the anodic reaction of a DMFC, methanol is oxidized, and protons, electrons and carbon dioxide are released. So far, platinum (Pt) is still the most popular catalyst for the methanol oxidation reaction (MOR). However, Pt is very easily poisoned by CO molecules, which are unavoidably produced during the electrooxidation of fuels and exist in reformed fuel gases. Reducing Pt usage for the commercialization of DMFCs is also important because of the high cost and low abundance of Pt. All factors necessitate the development of new catalytic systems to reduce Pt loading, increase catalytic activity and improve durability [8-9].

Tungsten carbide (WC) is widely used in mechanical processing because of its high hardness, high melting point, fracture resistance, wear resistance, oxidation resistance and corrosion resistance [10]. Since Levy and Boudart discovered its Pt-like catalytic property in 1973, WC has been used as a stable and alternative catalyst material for the dissociation of methanol and water [11]. Hwu [12] investigated the decomposition of methanol by carbide-modified W (111) and found that the surface of carbide has high activity for the decomposition of methanol. Yan [13] presented that WC could be used as an accelerator to improve the electrocatalytic activity of platinum and palladium catalysts in the methanol oxidation, oxygen reduction and hydrogen evolution reactions. Shi [14] synthesized Pt/Ru/WC/reduced graphene by the deposition redox replacement method. The results showed that the WC/RGO composite modified by Pt and Ru NPs can enhance the CO tolerance of Pt towards the MOR. Ham [15] synthesized Pt supported on mesoporous WC by the borohydride reduction method. The Pt/WC with low Pt loading showed much higher activity and improved resistance to CO poisoning. Zhao [16] used the organic colloidal method to synthesize Pt catalysts supported on WC/multi-walled carbon nanotubes. In this experiment, the performance of Pt catalysts for the MOR was enhanced significantly under the combined effect of Pt nanoparticles and WC. Sean T [17] demonstrated a self-assembly method to prepare Pt/WC nanoparticles, in which WC nanoparticles (<10 nm) were coated with atomically thin Pt monolayer surface shells. The core-shell materials showed superior catalytic activity and excellent stability with reduced Pt loading compared to state-of-the-art commercial catalysts for electrochemical applications, but the synthesis process was very complex.

Many new preparation methods, such as ion exchange [18], impregnation reduction [19], and colloidal methods [20], have been used to design and synthesize new electrocatalysts.

After heat treatment, the particle size is usually increased, and the catalytic activity is reduced. A multiple and repeated filtration and washing process appears in the ion exchange method, which leads to lower yields and increases the total cost of catalyst production [18]. The impregnation reduction of Pt precursors in high temperature hydrogen atmospheres has been extensively studied [19]. In the colloidal method, acid must be used to destroy the colloid and thus accelerate the deposition and agglomeration of metal particles [20]. Furthermore, the above preparation methods usually have two steps. The first step is generally to prepare catalyst supports such as nanocarbon or nano WC/C materials. The second step is usually to deposit metal particles on the catalyst supports. In this work, a one-pot method was developed to synthesize Pt/WC_x/nanocarbon catalysts. The Pt and WC form an alloy when introduced in an appropriate ratio. The as-prepared Pt/WC_x/nanocarbon electrocatalysts demonstrate significant enhancements of electrochemical performance towards the MOR.

2. EXPERIMENTAL

2.1 Materials

Materials used in this work include carbon black (Vulcan XC-72R, Cabot Corp.), concentrated sulfuric acid (H_2SO_4), concentrated nitric acid (HNO_3, XinDongShiJi company), PDDA ($(C_8H_{16}CIN)_n$) and hexachloroplatinic acid ($H_2PtCl_6 \cdot xH_2O$, Sigma-Aldrich), sodium tungstate dehydrate (STD, $Na_2WO_4 \cdot 2H_2O$, TianJinZhiYuan Reagent Co., Ltd), methanol (CH_3OH, Sinopharm Chemical Reagent Co., Ltd), and Nafion solution (5 wt.% in isopropanol and water, DuPont company).

2.2 Synthesis of the electrocatalysts

First, 0.2 g carbon black and 10 mL concentrated nitric acid were mixed in 30 mL concentrated sulfuric acid under ultrasonic treatment at 60°C for 2 h. The mixture was filtered and washed three times with deionized water. The filtration product and 4 mL PDDA (5 wt.% in water) were added into 100 mL deionized water under stirring at room temperature for at least 30 min. The as-obtained mixture was filtered and washed again with deionized water. The slurry was added into 100 mL deionized water, and then certain amounts of STD and H_2PtCl_6 were added.

The mass fractions of WC in the supporting materials (WC+Carbon) were set at 5%, 15% and 25%, respectively. The mass fraction of Pt was 5% in all three catalysts. The final products were labelled as Pt/$WC_{0.05}$/C, Pt/$WC_{0.15}$/C and Pt/$WC_{0.25}$/C, respectively. The above mixtures were freeze-dried completely, followed by slight grinding in an agate mortar. The powders were heated in a tube furnace for 30 min under an Ar-H_2 atmosphere at 1200°C and then cooled to room temperature.

2.3 Characterization

XRD data were obtained using an XRD-6000 diffractometer employing Cu Kα radiation under wide angle conditions of 10°-90° and 16 min. A scanning electron microscope with a field emission gun (FESEM, JEOL JSM-6340F) and EDS spectrum image were used to characterize the morphology, particle size distribution, and elementary composition. Raman spectra (Renishaw RW1000) were used to test the composition and structure of the as-prepared catalysts composite materials. Transmission electron microscopy (TEM) was used to observe the two-dimensional morphology of the catalysts. X-ray photoelectron spectroscopy with high resolution (XPS) is a common method to characterize the surface composition and structure of as-prepared catalysts under ultra-high vacuum.

A potentiostat/galvanostat (Autolab PGStat 30) was used to measure electrochemistry in a traditional three-electrode cell at room temperature. The working electrode used was a glassy carbon electrode (GCE, 5 mm diameter), the counter electrode was a platinum wire, and the reference electrode was silver chloride (Ag/AgCl). The salt bridge was connected to the reference electrode by a Lukin capillary. A uniform ink with a catalyst concentration of 5 mg ml^{-1} was formed by mixing electrocatalyst powder with isopropanol by ultrasonication, which was conducted in order to load the electrocatalyst suspension into GCE. Then, 10 μL of electrocatalyst ink was deposited onto the GCE

surface. Next, the electrocatalyst was immobilized by coating a drop of 0.5 wt% Nafion solution on the surface. The standard hydrogen electrode (SHE) was used as a reference electrode to calibrate all electrochemical potentials in this experiment. When the scan rate was 50 mV s^{-1} and the temperature of a N_2-purged 0.5 M H_2SO_4 + 1 M CH_3OH solution was 25°C, CV measurements were used to characterize the electrocatalytic activity for the MOR.

3. RESULTS AND DISCUSSION

It is well known that acid treatment can make the surfaces of carbon materials contain oxygen-containing groups such as hydroxyl, epoxy, carboxyl and carbonyl groups [21, 22]. The synthesis route of Pt/WCx/nanocarbon is shown in Fig. 1. Because negatively charged groups exist on the surface of carbon supports, the first step in self-assembly will occur after adding positively charged PDDA molecules [23]; then, the surface charge on the powders will transition to a positive charge. The above-mentioned results show that the negatively charged $PtCl_6^{2-}$ and WO_4^{2-} are self-assembled on the surfaces of carbon supports. Then, freeze drying was employed to remove the solvent molecules. After carbonization under an Ar-H_2 atmosphere at 1200°C for 2 h, uniformly distributed Pt nanoparticles alloyed with WC on the carbon supports were obtained.

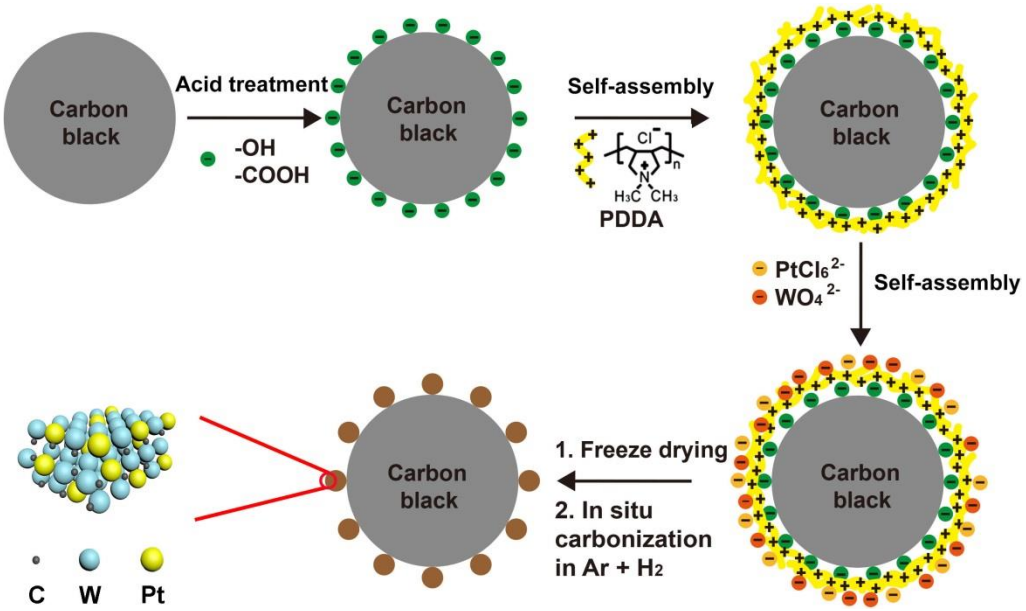

Figure 1. Schematic diagram of the synthesis of Pt/WC_x/C.

X-ray diffraction was used to determine the structure of the Pt/WC_x nanoparticles on the carbon supports. The average crystallite size of the Pt/WC_x nanoparticles can be calculated using the Scherrer equation:

$$t = 0.9\frac{\lambda}{\beta cos\theta_b}$$

where t is the crystallite size in Å, λ is the wavelength (1.5406 Å in this case for Cu Kα radiation), β is the full-width at half maximum (FWHM) of a peak in the XRD spectrum, and θ_b is the diffraction angle for that peak. The XRD patterns of the as-prepared electrocatalysts are shown in Fig. 2a. All the XRD patterns of Pt/$WC_{0.05}$/C, Pt/$WC_{0.15}$/C and Pt/$WC_{0.25}$/C have unambiguous characteristics of Pt (PDF#01-084-0640). The diffraction angles of 39.9°, 46.4° and 67.5° were assigned to the (111), (200) and (220) diffraction planes of Pt [24]. Pt/$WC_{0.25}$/C also showed the characteristic peaks of WC according to PDF#01-072-0097. The diffraction angles of 31.4°, 35.6° and 48.3° for Pt/$WC_{0.25}$/C were assigned to the (111), (200) and (220) diffraction planes of WC. In the Pt/$WC_{0.05}$/C and Pt/$WC_{0.15}$/C samples, no WC diffraction peaks were observed. The reason may be attributed to WC being amorphous and evenly dispersed in the Pt matrix. The EDS diagrams for the different composite electrocatalysts exhibited the characteristic peaks of elemental C, Pt and W as shown in Fig. 2b.

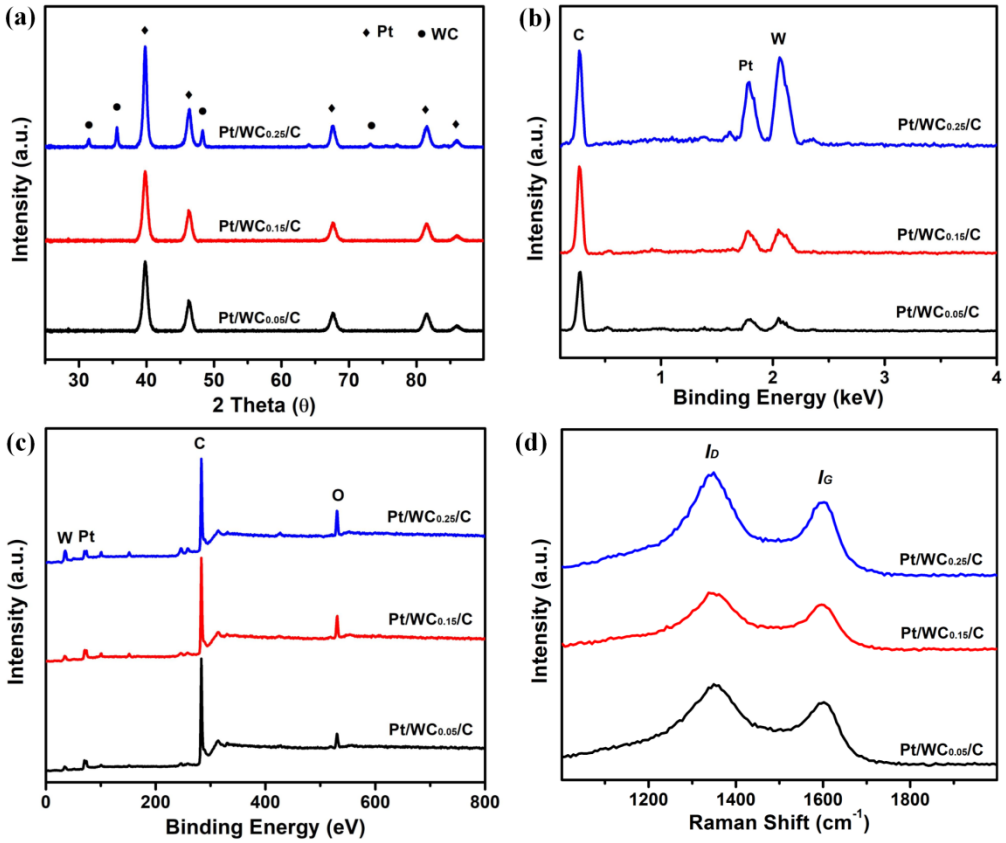

Figure 2. (a) XRD patterns, (b) EDS spectra, (c) XPS survey scan and (d) Raman spectra of Pt/$WC_{0.05}$/C; Pt/$WC_{0.15}$/C and Pt/$WC_{0.25}$/C.

The surface chemistry of the catalysts with carbon support was further studied by high resolution XPS. Elemental W, Pt, C and O were observed in the XPS spectrum in Fig. 2c. The W 4f peaks increased significantly with increasing WC content, which is consistent with the XRD results. The Raman spectra of the different catalysts are shown in Fig. 2d. It can be seen that the carbon in the supports has both graphite and non-graphite forms. The main peaks in the spectra are located at 1594 cm^{-1} (G band) and 1340 cm^{-1} (D band). First, the G band represents the E_{2g} vibration of graphitic carbon (electronic configuration is sp^2). Second, the D band represents the A_{1g} mode of diamond-like

carbon (electronic configuration is sp^3). The value of the G band (I_G) divided by the D band (I_D) is the relative intensity ratio, which can be used to evaluate the degree of carbon graphitization [25]. The I_G/I_D ratios of Pt/$WC_{0.05}$/C, Pt/$WC_{0.15}$/C and Pt/$WC_{0.25}$/C were 0.79, 0.82 and 0.69, respectively. The results indicate that the graphitization degrees of the three samples are similar.

Fig. 3 shows the FESEM images of the carbon black used in this work and different catalysts. Fig. 4 presents the TEM images of the different catalysts. As seen, the metal nanoparticles were mainly dispersed on the outer surface of carbon black, and there is no obvious agglomeration in the prepared electrocatalysts. The morphology and structure of carbon black as a supporting material did not show obvious change after loading Pt/WC_x catalysts, which indicated that there was no serious damage on the carbon black during the whole synthesis process. The Pt particle sizes in ETEK were approximately 2~4 nm. The particle sizes of the catalysts were all approximately 4~6 nm in the Pt/$WC_{0.05}$/C, Pt/$WC_{0.15}$/C and Pt/$WC_{0.25}$/C samples, which is in accordance with the crystalline sizes calculated by the Scherrer equation [26].

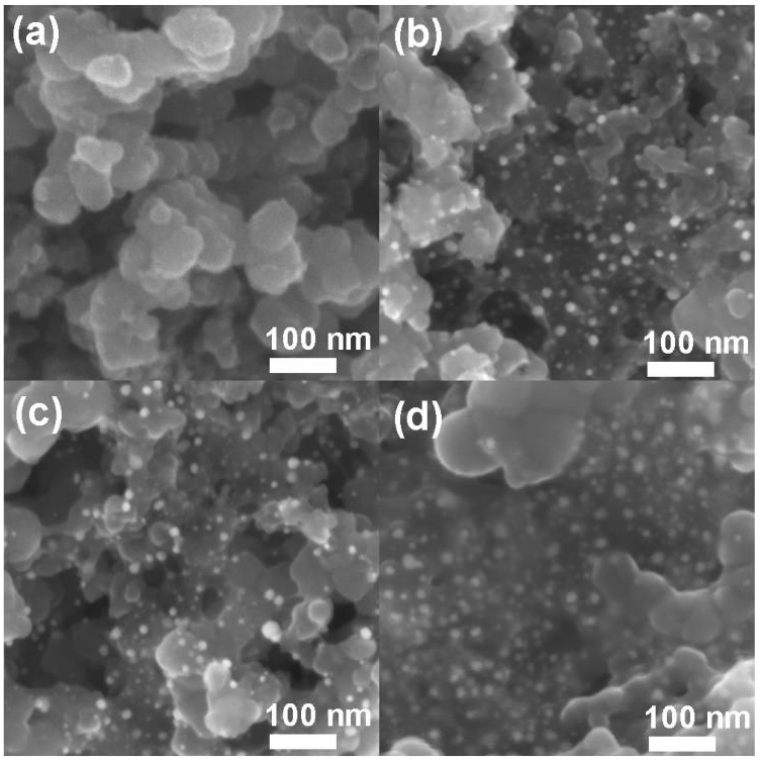

Figure 3. FESEM images of:(a) carbon black, (b) Pt/$WC_{0.05}$/C, (c) Pt/$WC_{0.15}$/C and (d) Pt/$WC_{0.25}$/C.

The XPS spectra of W 4f and Pt 4f of the catalysts were analysed to investigate the valence states of the Pt and W elements in Fig. 5. The deconvolution results are listed in Table 1. Based on the different areas of Pt $4f_{7/2}$ and W $4f_{7/2}$, the relative intensities of different species can be obtained [27]. The XPS peaks of the W 4f core level can be characterized as two doublets of W ($4f_{7/2}$) and W ($4f_{5/2}$) signals, which are shown in Fig. 5a. For Pt/$WC_{0.05}$/C, the first doublet with 32.01 and 34.14 eV binding energies was assigned to the XPS signals of the W^{4+} state in form of WC, while the second doublet with 35.65 and 37.75 eV binding energies was assigned to the W^{6+} state in form of WO_3 [28]. From

Table 1 we can see that the binding energy of the W^{6+} species shows a positive shift with increasing WC content, which may be attributed to electron transfer from W atoms to Pt atoms.

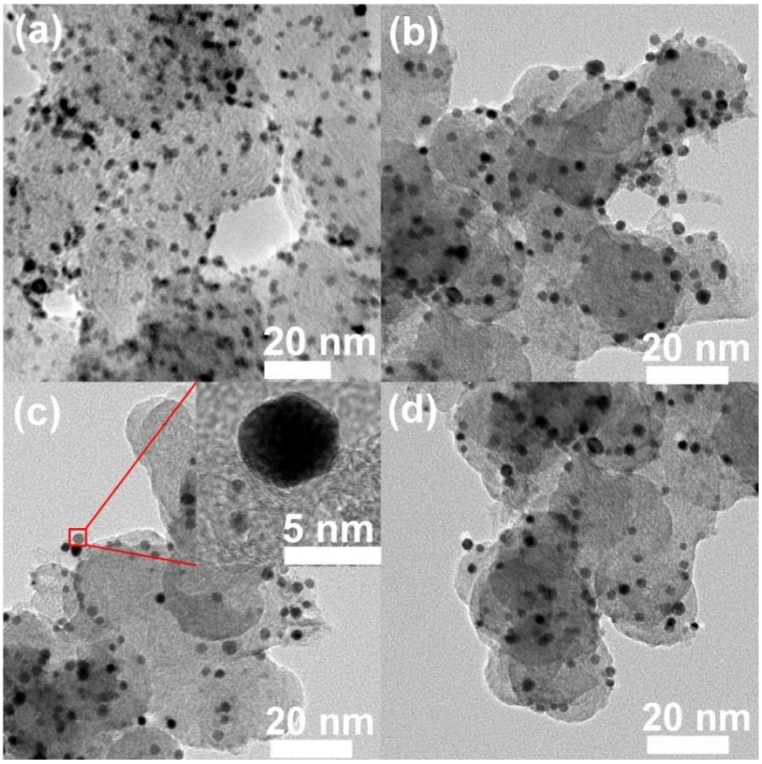

Figure 4. TEM images of: (a) ETEK, (b) Pt/$WC_{0.05}$/C, (c) Pt/$WC_{0.15}$/C with high magnification inset and (d) Pt/$WC_{0.25}$/C.

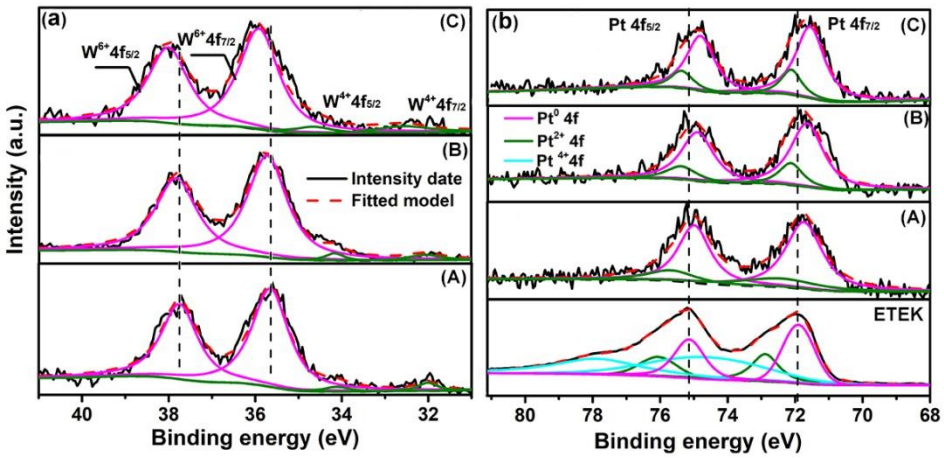

Figure 5. High resolution W 4f and spectra of: (A) Pt/$WC_{0.05}$/C, (B) Pt/$WC_{0.15}$/C and (C) Pt/$WC_{0.25}$/C and high resolution Pt 4f spectra of ETEK, (A) Pt/$WC_{0.05}$/C, (B) Pt/$WC_{0.15}$/C and (C) Pt/$WC_{0.25}$/C.

The relative intensities of W^{4+} are 4.30%, 4.13% and 8.41% for Pt/$WC_{0.05}$/C, Pt/$WC_{0.15}$/C and Pt/$WC_{0.25}$/C respectively. All the XPS peaks of Pt in the catalysts are doublet-like shapes consisting of Pt ($4f_{7/2}$) and Pt ($4f_{5/2}$) signals in Fig. 5b. For Pt/$WC_{0.05}$/C, the peaks located at 71.74 eV and 74.99 eV correspond to metallic Pt. The smaller peaks located at 73.02 eV and 75.27 eV correspond to the Pt^{2+} state in the forms of PtO and Pt_2W. In Table 1, the Pt^0 4f shows a negative shift relative to ETEK. When the electronic charge density of the Pt atoms increases, a negative shift in the binding energy will appear, which indicates that the electron has been transferred from the W atom to the Pt atom. As the D-band centre of platinum moves downward, the adsorption strength is usually weakened, which helps remove CO groups and improve the activity of the MOR [29].

Table 1. Binding energies and relative intensities of XPS spectra of Pt and W species in the catalysts

Catalyst	Species	Binding energy (eV)	Relative intensity (%)	Species	Binding energy (eV)	Relative intensity (%)
ETEK	Pt^0 $4f_{7/2}$	71.90	33.36			
	Pt^{2+} $4f_{7/2}$	72.90	18.37			
	Pt^{4+} $4f_{7/2}$	74.6	48.33			
Pt/$WC_{0.05}$/C	Pt^0 $4f_{7/2}$	71.74	78.51	W^{4+} $4f_{7/2}$	32.01	4.30
	Pt^{2+} $4f_{7/2}$	73.02	21.53	W^{6+} $4f_{7/2}$	35.65	95.71
Pt/$WC_{0.15}$/C	Pt^0 $4f_{7/2}$	71.57	80.25	W^{4+} $4f_{7/2}$	31.99	4.13
	Pt^{2+} $4f_{7/2}$	72.12	19.81	W^{6+} $4f_{7/2}$	35.73	95.90
Pt/$WC_{0.25}$/C	Pt^0 $4f_{7/2}$	71.55	80.33	W^{4+} $4f_{7/2}$	31.73	8.41
	Pt^{2+} $4f_{7/2}$	72.11	19.72	W^{6+} $4f_{7/2}$	35.91	91.60

In the N_2-saturated 0.5 M H_2SO_4 solution with or without 1.0 M CH_3OH solution, the results in Fig. 6 show that the electrocatalytic activity of different catalysts for MOR were investigated under conditions of 25° C. In a 0.5 M H_2SO_4 solution, the results in Fig. 6a show the electrochemical surface areas (ECSAs) of the electrocatalysts that were calculated by the hydrogen adsorption/desorption area in the CV curves [30,31]. Higher ECSAs give rise to more activation sites of hydrogen adsorption/desorption. These activation sites are excellent choices for both hydrogen oxidation and the MOR because hydrogen adsorption/desorption is also an important step for the MOR. Normally, the size of Pt catalysts particles will tend to decrease with increasing ECSA. The ECSA of the as-prepared catalysts was higher than that of ETEK, although their particle sizes are bigger than those of ETEK. The improvement in ECSA may benefit from the introduction of "Pt-like" WC [32]. The CV curves of the as-synthesized electrocatalysts and ETEK the MOR in acidic solution are compared and plotted in Fig. 6b. The peak current densities for the MOR on Pt/$WC_{0.05}$/C, Pt/$WC_{0.15}$/C and Pt/$WC_{0.25}$/C are 529.39, 552.40 and 430.03 mA mg^{-1}_{Pt}, respectively, while ETEK only shows 416.29 mA mg^{-1}_{Pt}. Under the same reaction conditions, WC without Pt possesses rather poor catalytic activity. Therefore, the WC activity will increase significantly under the coordination of Pt and WC. The WC surface has higher water decomposition activity than the Pt surface. Therefore, hydrogen is adsorbed on the surface of Pt, and then, it migrates to the WC surface under the effect of hydrogen spill over [8]. The

tolerance of CO on the platinum surface is calculated by the ratio of peak current of I_f (the forward peak current) to that of I_b (the reverse peak current). The higher the I_f/I_b ratio is, the higher the tolerance for CO [33]. The I_f/I_b ratios of as prepared catalysts are much higher than those of ETEK, as shown in Table 2. The results further show that the catalyst can significantly increase CO tolerance. Here, the promotion effect of WC is remarkable. The mechanism for improving performance can be revealed through the coordination of Pt and WC [34]. The reaction process of the MOR is very complicated, which is due to having many intermediate species. In electrochemical methanol oxidation and water decomposition [35], the active sites will be blocked to poison the Pt. Hydroxyl groups generated by water activation are crucial to remove metal-poisoned CO molecules on the catalyst surface. In addition, based on the d-band centre theory, CO adsorption will decrease as the centre of d-band decreases [36]. Therefore, under the effect of the negative shifting of d-band centres of Pt on catalysts, the adsorbed poisoning intermediates can be effectively removed, and CO can also be removed in the MOR [37]. The synthesis method and MOR performance of the current work were compared to relevant reports, as shown in Table 3. After a cyclic voltammetry investigation of the MOR, in order to research catalyst poisoning resistance, a CO stripping process experiment was conducted. In 0.5 M H_2SO_4 solution, the surface of the electrode should be treated by an electrochemical cleaning method with a potential cycling (0.2 – 1 V, 20 cycles) before the above-mentioned experiment was conducted. The results of CO stripping process are illustrated in Fig. 6c. A lower poisoning resistance to CO was found in the prepared catalysts. Under the same conditions [38], the CO desorption temperature on the WC surface was lower than that on the Pt surface. Therefore, the oxidation and desorption ability of the absorbed CO could be enhanced significantly by applying WC, which could further improve the catalyst poisoning resistance. In a N_2-saturated 0.5 M H_2SO_4+ 1 M CH_3OH solution, the stabilities of electrocatalysts were measured by chronoamperometry under the test conditions of 0.6 V for 7200 s. As shown in Fig. 6d, the current density decreased rapidly within 0~50 s due to the poisoning effect on the catalyst surface. After 50 s, the polarization current slowly decayed and eventually maintained a steady state. After polarizing at 0.6 V for 7200 s, the polarization currents for the MOR on ETEK, Pt/$WC_{0.05}$/C, Pt/$WC_{0.15}$/C, and Pt/$WC_{0.25}$/C are 107.82, 268.46, 134.97 and 109.83 mA mg^{-1}_{Pt}, respectively [39-40]. The current densities of Pt/$WC_{0.05}$/C, Pt/$WC_{0.15}$/C and Pt/$WC_{0.25}$/C were significantly higher than that of ETEK because of the synergistic effect between Pt and amorphous WC. That is, the Pt/$WC_{0.15}$/C catalyst displayed the best stability for the whole duration of the scan [41, 42].

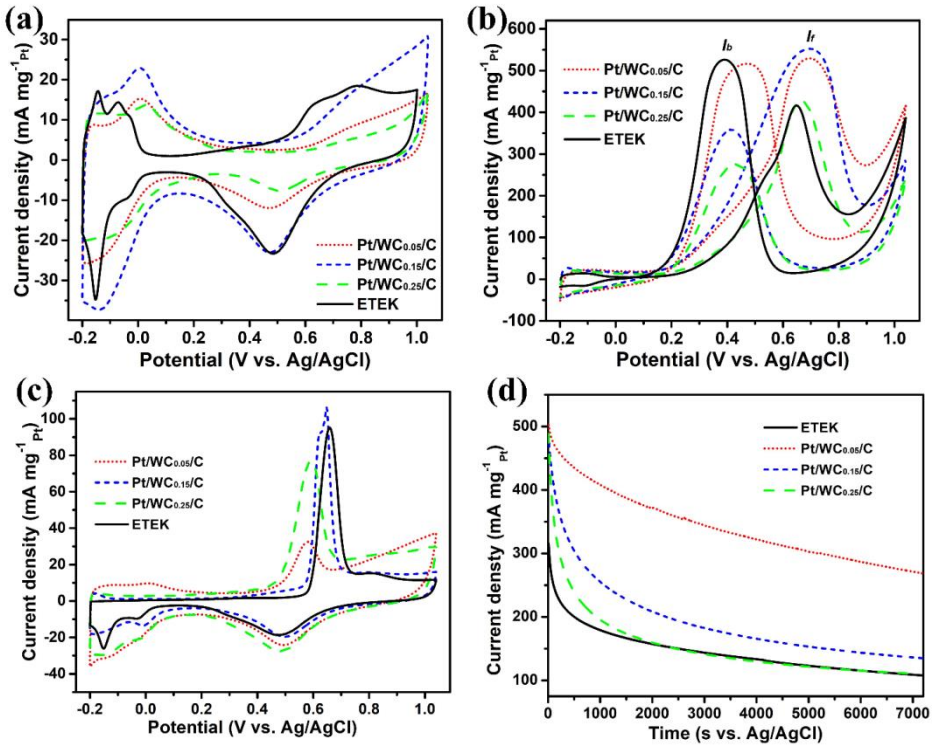

Figure 6. Cyclic voltammograms of the catalysts (a) in a N_2-saturated 0.5 M H_2SO_4 solution, (b) in a N_2-saturated 0.5 M H_2SO_4 + 1 M CH_3OaoH solution and (c) CO stripping voltammograms in a 0.5 M H_2SO_4 solution at 25°C with a scan rate of 50 mV s^{-1}, (d) CA curves of the catalysts in a N_2-saturated 0.5 M H_2SO_4+ 1 M CH_3OH solution at 25°C

Table 2. The properties and electrochemical parameters of the different catalysts.

Catalyst	ECSA (cm^2 mg^{-1}_{Pt})	Onset potential (V)	Peak potential (V)	Peak current (mA mg^{-1}_{Pt})	Ratio (I_f/I_b)
$Pt/WC_{0.05}/C$	224.84	0.15	0.70	529.39	1.03
$Pt/WC_{0.15}/C$	257.23	0.14	0.69	552.40	1.54
$Pt/WC_{0.25}/C$	215.71	0.19	0.67	430.03	1.59
ETEK	185.41	0.22	0.66	416.29	0.85

Table 3. Comparisons of the MOR performance for Pt based catalysts in recently published papers.

Reference	Catalyst	ECSA (cm^2 mg^{-1}_{Pt})	Ratio (I_f/I_b)	Methods
25	Pt/NOMC-3D	402	1.1	nanocasting method
30	$Pt/C/TiO_2$	266	1.01	a step-wise mechanical and plasma sputtering method
31	PtRu nanodendrites	290	1.66	one-pot method
32	PtPb alloy	570	1.23	microwave heating method
39	Pt/TiN	529	1.01	hydrothermal method
40	Pt/CNT	197	—	solid phase reaction method
Current work	$Pt/WC_{0.15}/C$	257.23	1.54	one-pot method

4. CONCLUSION

In brief, $Pt/WC_x/C$ electrocatalysts were successfully prepared by the one-pot method. The preparation process did not cause obvious damage to the surfaces of the carbon materials, and the graphitization degrees of the three samples were similar. The $Pt/WC_{0.15}/C$ catalyst displayed the highest activity and best stability towards MOR. Significant enhancements of electrochemical performance were attributed to the negative shift of the d-band centre of Pt and synergistic effects between Pt and WC. This one-pot method can be used to manufacture a variety of nanohybrid electrocatalysts. The $Pt/WC_{0.15}/C$ electrocatalyst is very promising for MOR applications in fuel cells.

ACKNOWLEDGEMENTS
This work was supported by the National Natural Science Foundation of China (51774177), the Natural Science Foundation Guidance Program of Liaoning Province (20170540468), the Liaoning Bai Qian Wan Talents Program (2017-104), the Program of Distinguished Professor of Liaoning Province (2017-60), the Project of Department of Education of Liaoning Province (2017LNQN14), and Innovative Research Team Funding of USTL (No. 2016TD05).

References

1. T. Elmer, M. Worall, S. Wu and S.B. Riffat, *Renew. Sust. Energ. Rev*, 42 (2015) 913.
2. S. Kattel, B. Yan, J.G. Chen and P.J. Liu, *J. Catal*, 343 (2016) 115.
3. G. Che, B.B. Lakshmi, C.R Martin, E.R. Fisher, *Langmuir*, 15 (1999) 750.
4. M. Sakthivel, A. Schlange, U. Kunz and T. Turek, *J. Power Sources*, 195 (2010) 7083.
5. X. Zhao, M. Yin, L. Ma, C. Liu, J. Liao, T. Lu and W. Xing, *Energ. Environ. Sci.*, 4 (2011) 2736.
6. J. Liu and S.A. Barnet, *Solid State Ionics*, 158 (2003) 11.
7. Z. Li, C. He, M. Cai, S. Kang and P.K. Shen, *Int. J. Hydrogen Energy*, 37 (2012) 14152.
8. J.l. Lu and Z.H. Li, *J. Power Source*, 202 (2012) 56.
9. Y.H. Li, L. Han, B. An, Y. Wang, L. Wang, X. Yin and J.L. Lu, *J. Mater. Sci*, 27 (2016) 6208.
10. J.W. Guo, T.S. Zhao, J. Prabhuram, R. Chen and C.W. Wong, *Electrochim. Acta*, 51 (2006**)** 754.
11. H. Chhina, S. Campbell and O. Kesler, *J. Power Sources*, 164 (2007**)** 431.
12. H.H. Hwu, B.D. Polizzotti and J.G. Chen Potention, *J. Phys. Chem. B*, 105 (2001**)** 10045.
13. Z. Yan, G. He, M. Cai, H. Meng and P.K. Shen, *J. Power Sources*, 242 (2013**)** 817.
14. J. Zhang, J. Chen, Y. Jiang, F. Zhou, G. Wang and R. Wang, *Appl. Surf. Sci.*, 389 (2016) 157.
15. H.D. Jin, Y.K. Kim, S.H. Han and J.S. Lee, *Catal. Today*, 132 (2008) 117.
16. Z. Zhao, X. Fang, Y. Li, Y. Wang, P.K. Shen, F. Xie and X. Zhang, *Electrochem. Commun*, 11 (2009) 290.
17. S.T. Hunt, M. Milina, A.C. AIba-Rubio, C.H. Hendon, J.A. Dumesic and Y. Román-Leshkov, *Catalysts*, 352 (2016) 974.
18. Y. Shao, G. Yin, J. Wang, Y. Gao and P. Shi, *J. Power Sources*, 161 (2006) 47.
19. S.R. De Miguel, O.A. Scelza, M.C. Román-Martínez, C. Salinas-Martínez de Lecea, D. Cazorla-Amorós and A. Linare-Solano, *Appl. Catal, A*, 170 (1998) 93.
20. Z. Zhou, S. Wang, W. Zhou, G. Wang, L. Jiang, W. Li, S. Song, J. Liu, G. Sun and Q. Xin, *Chem. Commun*, 39 (2003) 394.
21. W. Zhou, Z. Zhou, S. Song, W. Li, G. Sun, P. Tsiakaras and Q. Xin, *Appl. Catal, B*, 46 (2003) 273.
22. D.V. Esposito and J.G. Chen, *Energy Environ. Sci.*, 4 (2011) 3900.
23. I.D. Rosca, F. Watari, M. Uo and T. Akasaka, *Carbon*, 43 (2005) 3124.

24. Z.S. Li, S.H. Xu, Y.X. Xie, Y.L. Wang and S. Lin, *Electrochim Acta*, 264 (2018) 53.
25. G.F. Long, X. H. Li, K. Wan, Z.X. Liang and J.H. Piao, *Appl. Catal. B-Environ*, 203 (2018) 541.
26. X.L. Chen; W.S. Li; C.L. Tan; W. Li; Y.Z. Wu, *J. Power Sources*, 184 (2008) 668.
27. Y.Q. Zhang, Y.L. Shi, R. Chen, L. Tao, C. Xie, D.D. Liu, D.F. Yan and S.Y. Wang, *J.Mater Chema A*, 6 (2018) 23028.
28. Y. Xiang, S. Lu and S. Jiang, *Chem. Soc. Rev*, 41 (2012) 7291.
29. S. Wang, S. Jiang and X. Wang, *Nanotechnology*, 19 (2008) 265601.
30. N. Su, X.L. Hu, J.B. Zhang, H.H. Huang, J.X. Cheng, J.C. Yu and C. Ge, *Appl. Surf. Sci*, 399 (2017) 403.
31. S.L. Lu, K. Eid, D.H. Ge, J.Guo, L. Wang, H.J. Wang and H.W. Gu, *J. Nam*, 00 (2013) 1.
32. M.S. ÇÖgenli and A.B. Yurtcan, *Int. J. Hydrogen. Energ*, 43 (2018) 10698.
33. V. Glibin, L. Svirko, I. Bashtan-Kandybovich and D. Karamanev, *Appl. Surf. Sci*, 604 (2010) 500.
34. A.L. Stottlemyer, E.C. Weigert and J.G. Chen, *Ind. Eng. Chem. Res*, 50 (2011) 16.
35. B. Hammer and J.K. Nørskov, *Surf. Sci.*, 359 (1996) 306.
36. D. Wang; S. Lu; Y. Xiang; S.P. Jiang, *Appl. Catal. B*, 103 (2011) 311.
37. Y.C. Kimmel; D.V. Esposito; R.W. Birkmire; J.G. Chen, *Int. J. Hydrogen Energy*, 37 (2012) 3019.
38. M.K. Jeon, K.R. Lee, W.S. Lee, H. Daimon, A. Nakahara and S.I. Woo, *J. Power Sources*, 185 (2008) 927.
39. W.Y. Li, Z.C. Pan, Z.J. Huang, Q.M. Zhou, Y.B. Xu, S.K. Wu, C. Chen, Y.S. Lin and G.H. Hu, *Int. J. Hydrogen. Energ*, 43 (2018) 9777.
40. X. Li, L. Luo, F. Peng, H.J. Wang and H. Yu, *Appl. Surf. Sci*, 434 (2018) 534.
41. J.L. Lu, S. Lu, D. Wang, M. Yang, Z. Liu, C. Xu and S.P. Jiang, *Electrochim. Acta*, 54 (2009) 5486.
42. L. Tao, S. Dou, Z. Ma and S. Wang, *Electrochim. Acta*, 157 (2015) 46.